NANO LETTERS

pubs.acs.org/NanoLett

Letter

One-Pot Synthesis of Affordable Redox-Responsive Drug Delivery System Based on Trithiocyanuric Acid Nanoparticles

Elena Kopoleva,▲ Maksim D. Lebedev, Alisa Postovalova, Anna Rogova, Landysh Fatkhutdinova, Olga Epifanovskaya, Alexander A. Goncharenko, Arina V. Kremleva, Nadezhda Domracheva, Anton S. Bukatin, Albert R. Muslimov, Aleksandra Koroleva, Evgeniy V. Zhizhin, Kirill V. Lepik, Alexander S. Timin, Oleksii Peltek,*▲ and Mikhail V. Zyuzin

Cite This: *Nano Lett.* 2023, 23, 10811−10820

Read Online

ACCESS | Metrics & More | Article Recommendations | Supporting Information

ABSTRACT: Redox-responsive drug delivery systems present a promising avenue for drug delivery due to their ability to leverage the unique redox environment within tumor cells. In this work, we describe a facile and cost-effective one-pot synthesis method for a redox-responsive delivery system based on novel trithiocyanuric acid (TTCA) nanoparticles (NPs). We conduct a thorough investigation of the impact of various synthesis parameters on the morphology, stability, and loading capacity of these NPs. The great drug delivery potential of the system is further demonstrated *in vitro* and *in vivo* by using doxorubicin as a model drug. The developed TTCA-PEG NPs show great drug delivery efficiency with minimal toxicity on their own both *in vivo* and *in vitro*. The simplicity of this synthesis, along with the promising characteristics of TTCA-PEG NPs, paves the way for new opportunities in the further development of redox-responsive drug delivery systems based on TTCA.

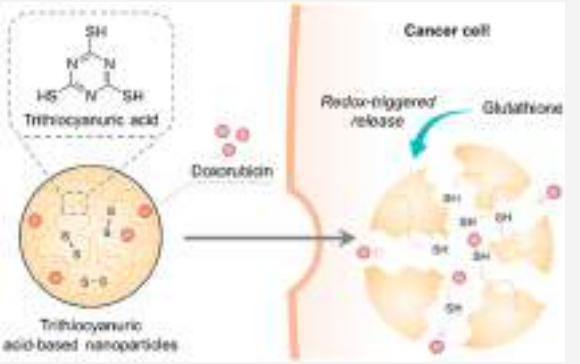

KEYWORDS: *redox-responsive nanoparticles, drug delivery, glutathione-responsive nanoparticles, trithiocyanuric acid*

Stimuli-responsive drug delivery systems offer promising clinical applications due to their ability to significantly alter the pharmacokinetics and release of bioactive compounds at regions of interest in response to specific exogenous or endogenous stimuli.[1] Most commonly utilized stimuli include temperature,[2,3] magnetic field,[4,5] light,[6] ultrasound,[7] pH gradient,[8] presence of enzymes,[9,10] etc. Among these, redox-responsive systems have attracted particular attention for their great promise in cancer treatment, due to their stability in normal tissues as a result of significant difference in redox potential between tumor and healthy cells,[11] fast response to increased concentrations of glutathione (GSH) in tumor cells,[6] and in some cases capability of enhancing endosomal escape,[12] which leads to an increased delivery efficiency.

Most extensively studied redox-responsive systems employ materials with disulfide bonds.[13−17] Such systems can be categorized into two groups: those which include disulfide bonds in their main monomers and those which use disulfide-containing moieties as linkers.[17] The former are of particular interest, since they are capable of depolymerization at a faster rate than other types of redox-responsive carriers, but in general they are less stable and are hard to modify.[11] The latter, on the other hand, require additional complex multistage processes during their synthesis, making it costly and complicated.[18−20]

In this context, we explore the use of trithiocyanuric acid (TTCA) as a promising material for the synthesis of redox-responsive carriers. This molecule has three thiol groups, which enables synthesis of three-dimensional particles through polycondensation with mild oxidants[21] or cross-linking agents,[22−24] that due to the abundance of disulfide bonds are susceptible to rapid degradation in the presence of GSH. Furthermore, TTCA is affordable compared to other thiol-rich polymers, since it is commonly used for heavy metal ion extraction,[21,25−27] while its potential for use in biomedical applications remains unexplored. This makes TTCA appealing when it comes to the translation of this technology into clinical practice.

In this study, we lay the groundwork for future research dedicated to the use of TTCA-based redox-responsive drug delivery systems. We propose methods for the synthesis of polymeric nanoparticles (NPs) from TTCA, which do not

Received: August 3, 2023
Revised: November 9, 2023
Accepted: November 13, 2023
Published: November 21, 2023

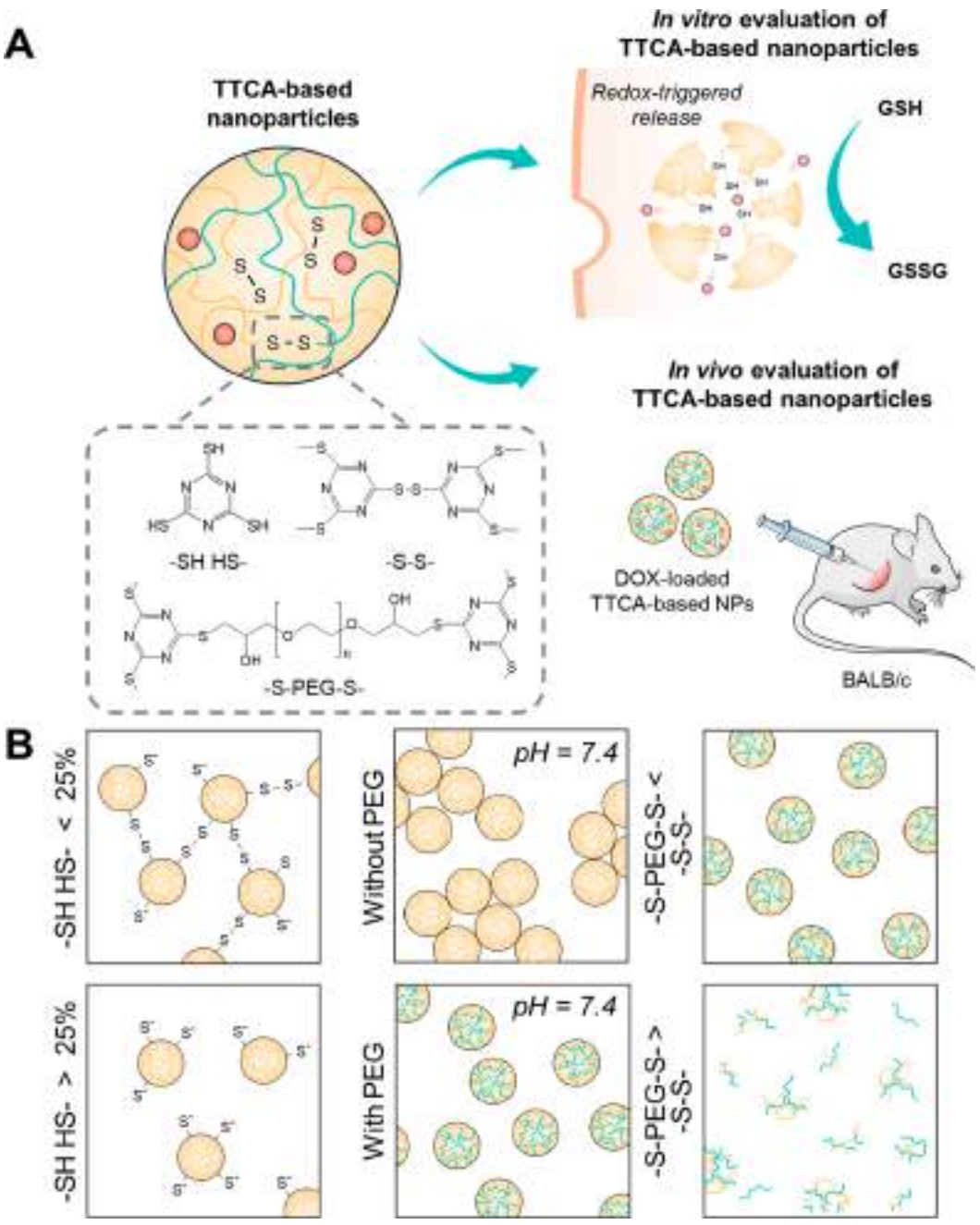

Figure 1. (A) Schematic illustration which outlines the main parts of this work. (B) Main synthesis parameters that determine the resulting properties of TTCA-based nanoparticles. The graphic was prepared using modified art elements from Servier Medical Art, found at https://smart.servier.com, used under a Creative Commons Attribution 3.0 Unported License.

include any complicated multistage processes of monomer premodification, thus offering a streamlined and cost-effective alternative to existing redox-responsive systems. We provide a thorough investigation into the effects of various synthesis parameters on the morphology and properties of the developed NPs. We believe that the obtained research outcomes will help to facilitate the further study of these developed NPs by other research groups.

The efficacy of TTCA NPs as redox-sensitive delivery systems is demonstrated through *in vitro* and *in vivo* experiments (Figure 1A). For instance, we explore cellular toxicity and uptake and examine particle *in vivo* biodistribution and histological changes of the main tissues. Additionally, we demonstrate the therapeutic efficacy of drug-loaded NPs for the treatment of breast cancer to highlight the potential of their clinical application.

Synthesis of TTCA NPs. At first, we investigated how various synthesis parameters affect the resulting properties of TTCA-based drug delivery systems, such as size, stability, and loading capacity. TTCA NPs were synthesized by utilizing a polycondensation method with mild oxidizers. Specifically, iodine was selected as the oxidizer, which was dissolved in a sodium iodide solution to obtain a homogeneous water-based solution. The NP synthesis was achieved in a straightforward, single-step process by adding iodine to the TTCA solution under consistent stirring. The resulting NPs were then isolated through centrifugation, followed by several water washes to

https://doi.org/10.1021/acs.nanolett.3c02933
Nano Lett. 2023, 23, 10811−10820

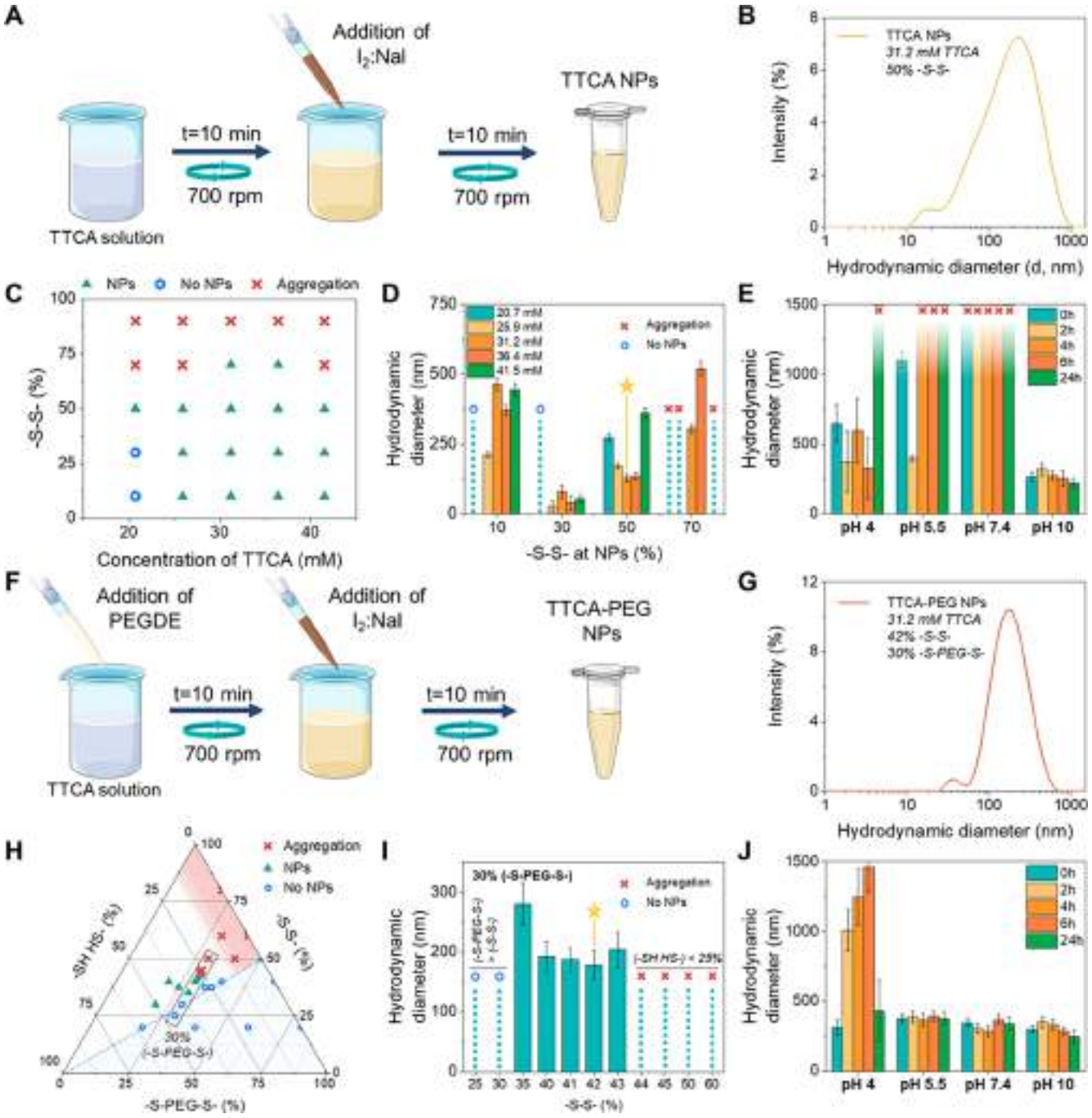

Figure 2. Optimization of synthesis. (A) Schematic illustration of TTCA NP synthesis. (B) Hydrodynamic diameter of TTTCK NPs with 50% −S−S− at 31.2 mM TTCA. (C) Result of the synthesis, depending on the calculated percentage of −S−S− bonds and the amount of TTCA. (D) Dependence of the hydrodynamic diameter of TTCA NPs as a function of the percentage of oxidized −SH groups and the amount of TTCA. (E) Time dependence of the hydrodynamic diameter of TTCA NPs on the pH of the buffer solution. (F) Schematic illustration of TTCA-PEG NP synthesis. (G) Hydrodynamic diameter of TTCA-PEG NPs with 30% −S−S− and 42% −S−PEG−S− bonds. (H) Result of the synthesis, depending on the calculated percentage of −S−S− and −S−PEG−S− bonds. (I) Hydrodynamic diameter of TTCA-PEG NPs as a function of the percentage of formed −S−S− (range from 25 to 60%) and 30% −S−PEG−S− bonds. (J) Time dependence of the hydrodynamic diameter of TTCA-PEG NPs on the pH of the buffer solution. All error bars represent the standard deviations determined from three independent assays. The graphic was prepared using modified art elements from Servier Medical Art, found at https://smart.servier.com, used under a Creative Commons Attribution 3.0 Unported License.

eliminate residual sodium iodine and unreacted TTCA monomers (Figure 2A).

The TTCA and iodine concentration were key parameters that varied during the synthesis, resulting in various ratios of TTCA thiol and disulfide groups.[28] Hence, by adjusting the oxidant and initial monomer concentrations, we obtained particles with different hydrodynamic diameters. We set the TTCA concentration to range from 20 to 45 mM, and the calculated percentage of thiol groups being oxidized into disulfide bonds varied from 10 to 90%, in increments of 20%.

https://doi.org/10.1021/acs.nanolett.3c02933
Nano Lett. 2023, 23, 10811−10820

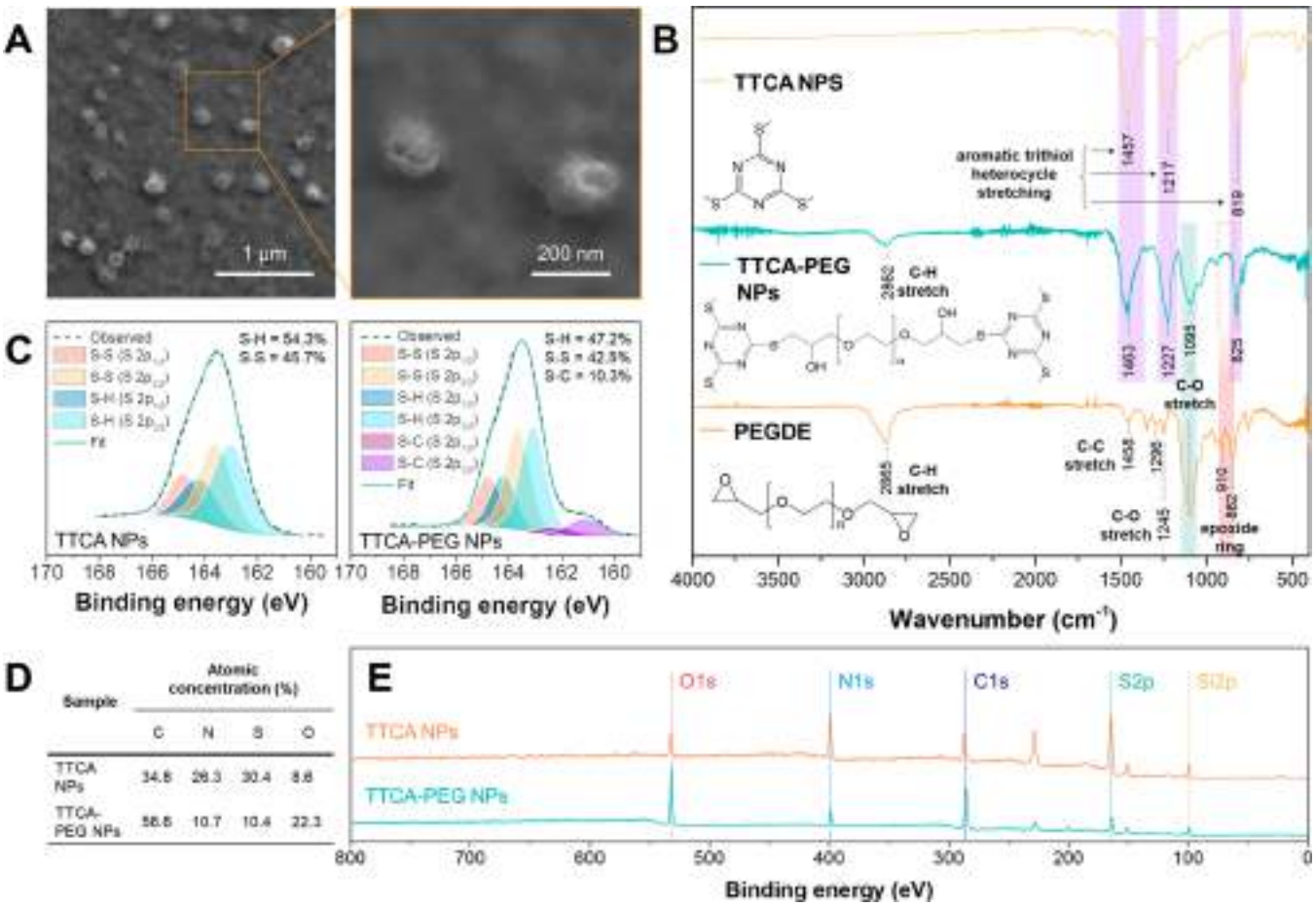

Figure 3. Structural characterization of TTCA and TTCA-PEG NPs. (A) Scanning electron microscopy (SEM) images of TTCA-PEG NPs. (B) Fourier transform IR spectra of TTCA, PEGDE, and TTCA-PEG NPs. On the spectrum of TTCA NPs, three prominent peaks are evident at 1457, 1217, and 819 cm^{-1}, which correspond to N−C−N and C−S bonds[34] in the heterocycle. In the PEGDE spectrum, the peak at 1095 cm^{-1} is indicative of C−O aliphatic ether, and peaks at 1296, 910, and 862 cm^{-1} relate to various vibrations of the epoxy group. The broad peak at 2867 cm^{-1} corresponds to vibrations of aliphatic CH_2 fragments. As for the spectrum of our synthesized NPs, vibrations related to the aromatic trithiocyanuric form are apparent at 1456, 1227, and 825 cm^{-1}, which can be assigned to C−N and C−S vibrations.[36] (C) XPS spectra of TTCA and TTCA-PEG NPs enlarged in different regions. (D) Atomic concentration on the surface of TTCA and TTCA-PEG NPs. (E) Overview of the XPS spectra of TTCA and TTCA-PEG NPs.

This percentage was estimated by first determining the quantity of thiol groups that would exist in an oxidized state and then dividing this value by the total number of thiol groups present. To calculate this, we assumed that all iodine reacted with all available thiol groups present in synthesis (Supporting Information section 2.1). We acknowledge that this assumption may represent a coarse approximation; however, we believe that it simplifies the explanation and interpretation of our results.

The verification of TTCA NPs formation and stability was assessed using dynamic light scattering (DLS), as depicted in Figure 2B. It was observed that a calculated disulfide percentage exceeding 70% led to substantial sample aggregation, which was confirmed by a rapid increase in hydrodynamic diameter of NPs. Conversely, low TTCA concentrations coupled with minimal iodine amounts resulted in no observable formation of TTCA NPs (Figure 2C,D). Furthermore, these synthesis conditions corresponded to extremely low yields of NPs relative to the initial monomer amount.

Based on these findings, the optimal conditions for TTCA NP synthesis were identified: TTCA at a concentration of 31 mM with 50% of the thiol groups forming disulfide bonds. The size distribution of these NPs obtained using DLS is depicted in Figure 2B, demonstrating a polydispersity index (PDI) of 0.289 and a zeta potential of −4.83 mV. The NPs exhibited excellent stability in water, with no significant changes in hydrodynamic diameter distribution over extended storage periods (Figure S1).

Given the envisioned application of TTCA NPs as drug delivery systems, their colloidal stability in physiological fluids is critical to prevent aggregation or disintegration within the body.[29] The NPs were therefore subjected to stability testing in different buffers. Figure 2E illustrates the change in hydrodynamic diameter over a 24 h period, showing that the TTCA NPs tended to aggregate in all buffers, except for alkaline buffers due to the ionic form of the −SH groups.[30] This can be explained by screening of the charges on the NP surface by ions present in buffers, which leads to a loss of their colloidal stability.[31]

Synthesis of TTCA-PEG NPs. To enhance the stability of TTCA NPs at neutral pH, we incorporated poly(ethylene glycol) diglycidyl ether (PEGDE) into NPs. PEGDE possesses epoxy groups that can readily react with the thiol groups of

https://doi.org/10.1021/acs.nanolett.3c02933
Nano Lett. 2023, 23, 10811−10820

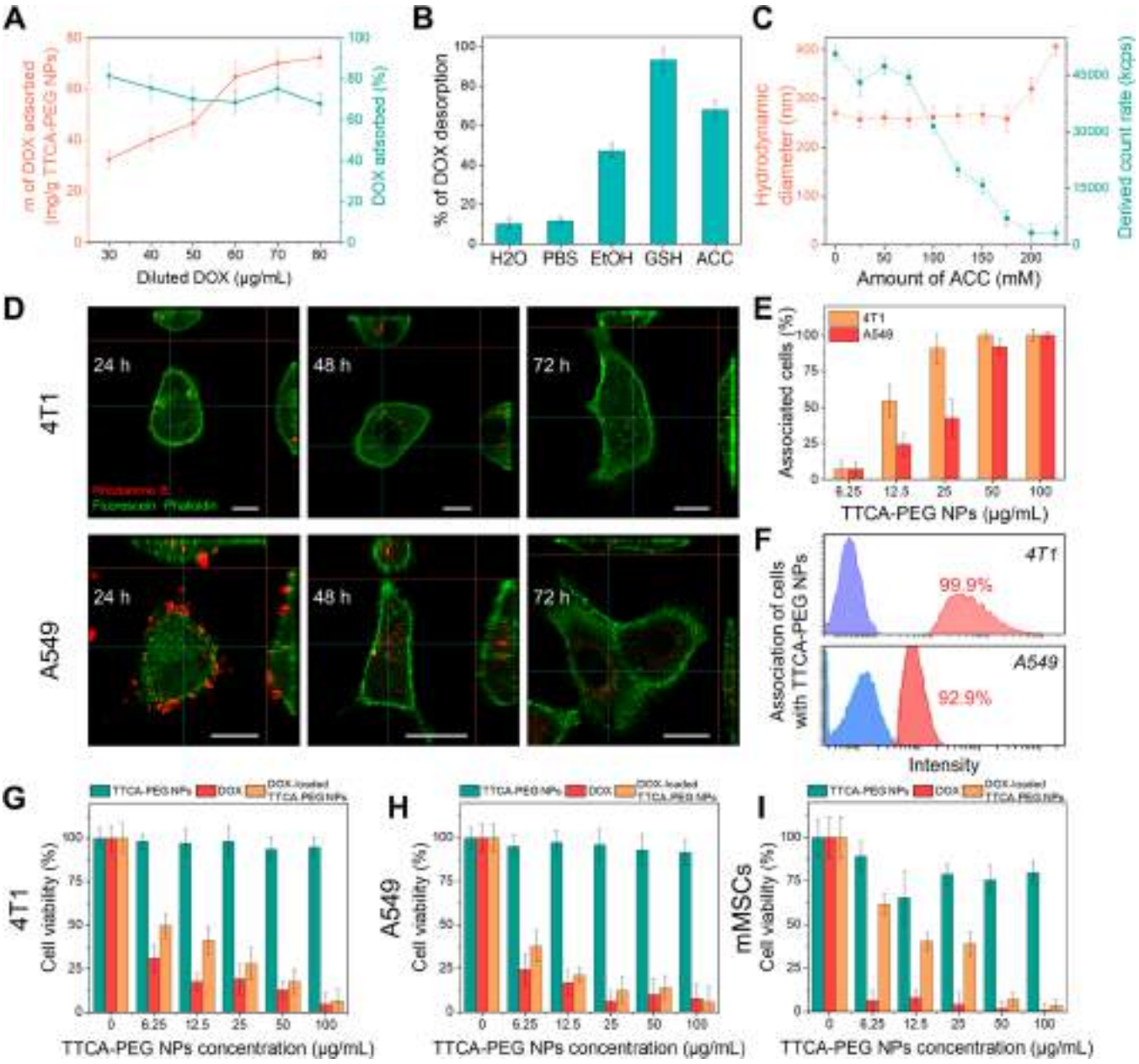

Figure 4. *In vitro* experiments. (A) Mass and percentage of adsorbed DOX on the surface of TTCA-PEG NPs depending on the initial concentration of DOX in solution. (B) Percentage of DOX desorption from the surface of TTCA-PEG NPs in solvents (water, PBS, ethanol, GSH, and ACC). The release of DOX was assessed spectrophotometrically after 60 min of incubation in different media. (C) Hydrodynamic diameter of TTCA-PEG NPs and count rate as a function of increasing percentage of 250 mM ACC solution in 25 mM increments. (D) Image of 4T1 and A549 cells stained with phalloidin labeled with fluorescein (λ_{ex} = 490 nm, λ_{em} = 525 nm) from a confocal microscope taken at different time points. Red fluorescence comes from RhB-labeled TTCA-PEG NPs (λ_{ex} = 546 nm, λ_{em} = 568 nm). The scale bar corresponds to 2 μm. (E) Distribution of fluorescence intensity of 4T1 and A549 cells incubated with RhB-loaded TTCA-PEG NPs added at different concentrations (6.25, 12.5, 25, 50, and 100 μg/mL). (F) Representative data of cell association with RhB-labeled TTCA-PEG NPs obtained using flow cytometry at 50 μg/mL. Cell viability of 4T1 (G), A549 (H), and mMSC (I) cells incubated with DOX, TTCA-PEG NPs, and DOX-loaded TTCA-PEG NPs added at various concentrations. Pure DOX was added at the same concentration as for DOX-loaded NPs, and TTCA-PEG NPs were added at the same amount as for DOX-loaded NPs. All error bars represent the standard deviation determined from three independent assays.

TTCA via a thiol-epoxy "click" chemistry reaction.[32] Furthermore, it also contains a polyethylene glycol (PEG) moiety commonly employed to boost the solubility of nanoformulations.[33]

The TTCA-PEG NPs were synthesized similarly to the TTCA NPs. Briefly, the TTCA solution was mixed with the PEGDE solution under constant stirring for 10 min, forming the TTCA-PEG compounds. Finally, addition of iodine solution resulted in the formation of NPs (Figure 2H).

After the synthesis of TTCA-PEG NPs, we suggest that TTCA molecules exist in one of three primary states: −S−S− (after reaction with I_2), −S−PEG−S− (following thiol−epoxy polymerization with PEGDE),[32] and −SH HS− (unreacted) (Figure 1A). While the TTCA concentration remained constant, the amounts of iodine and PEGDE introduced

https://doi.org/10.1021/acs.nanolett.3c02933
Nano Lett. 2023, 23, 10811−10820

varied. A summary of the synthesis process is illustrated in Figure 2H. The proportions of these three states were calculated similarly to Figure 2C. Essentially, the amount of thiol groups in oxidized form was divided by the total amount of thiol groups participating in a reaction, assuming that the reaction of thiols with PEGDE or I_2 had a 100% yield (Supporting Information section 2.2). Although this is a rough estimation, we believe that it simplifies the explanation of results and their interpretation.

Interestingly, no NPs were observed when the calculated percentage of −S−PEG−S− bonds exceeded that of the −S−S− bonds. We hypothesize that the slight hydrophobicity of the polycondensed TTCA complexes aids the formation of NPs, while the addition of highly soluble polyethylene glycol (PEG) hinders NPs formation. Moreover, syntheses yielding less than 25% calculated −SH HS− often resulted in aggregates, possibly due to the necessity of having free thiol groups on the NP surface to provide surface charge (Figure 1B).

Considering these observations, we set the amount of calculated −S−PEG−S− groups at 30% and varied the amount of iodine. Noticeably, once the calculated amount of −S−S− bonds exceeds 30% of −S−PEG−S−, we observed no NPs after centrifugation (Figure 2I). Furthermore, once the total amount of −SH HS− groups becomes less than 25%, it leads to the formation of aggregates. Ultimately, we selected the TTCA-PEG NP synthesis with 30% −S−S− and 42% −S−PEG−S_, showcasing a hydrodynamic diameter of 174 nm, PDI = 0.291, and ζ-potential −29.3 mV for further study (Figure 2G).

Akin to the case for TTCA NPs, we evaluated the colloidal stability by measuring hydrodynamic diameters in buffers with different pH levels over 24 h (Figure 2J). The decrease in hydrodynamic diameter of TTCA-PEG NPs after 24 h in acidic buffer (pH = 4.0, Figure 2J) can be explained by the significantly high aggregation of NPs, which leads to lower quality data obtained using DLS spectroscopy. Compared to TTCA NPs, TTCA-PEG NPs exhibited significantly improved stability, which made it possible to explore their interaction with cells *in vitro*.

Structural characterization of TTCA-PEG NPs. The TTCA and TTCA-PEG NPs synthesized under different conditions were visualized using scanning electron microscopy (SEM) and transmission electron microscopy (TEM), as depicted in Figure 3A and Figures S3 and S5. The images reveal TTCA NPs with diameters of less than 200 nm, which mirrors previous DLS data.

Infrared (IR) spectroscopy served as a further tool to validate the chemical structure of synthesized TTCA-PEG NPs. On the IR spectra of the synthesized TTCA-PEG NPs (Figure 3B) can be seen the double peak at 1090 and 1035 cm^{-1} relating to C−O aliphatic ether, and the 2867 cm^{-1} peak corresponds to CH_2 fragments of PEG. The presence of aliphatic ether, as well as the lack of vibrations associated with epoxy groups (1296, 910, and 862 cm^{-1}),[35] confirms a successful bond formation between TTCA and PEGDE.

X-ray photoelectron spectroscopy (XPS) was used to examine the chemical composition and bonding states of the surfaces of the investigated materials. The observed atomic content and peaks of C 1s, N 1s, and S 2p are consistent with the chemical composition of the TTCA polymer particles (Figure 3D,E). In the high-resolution spectra of S 2p, sulfur was present in triazine moieties within S−S disulfide bond states (~45%) and in the thiol form SH (~55%) (Figure 3C).[37] These results align with the calculated percentage of −S−S− groups for this synthesis (Figure 2B).

The atomic content of C 1s and O 1s for TTCA-PEG NPs increased compared with that of TTCA NPs, reflecting the incorporation of polyethylene glycol molecules into the NP structure. Notably, an additional peak appeared in the high-resolution S 2p spectra of TTCA-PEG, indicative of an S−C bond (~10%).[37,38] This observation confirms the covalent attachment of polyethylene glycol to TTCA. It should be noted that while the −S−C− group itself is not redox-responsive, the overall abundance of −S−S− bonds in the TTCA-PEG NP structure ensures complete degradation of the NPs in the presence of GSH.

However, the observed proportion of S−C bonds does not match the initially calculated amount of −S−PEG−S− groups. This discrepancy further supports the hypothesis regarding the high solubility of the TTCA-PEG complexes formed during the initial synthesis step before the addition of I_2. We assume that TTCA molecules bonded with 2 or 3 PEGDE molecules did not contribute to the formation of TTCA-PEG NPs, resulting in a lower TTCA-to-PEG ratio in the final TTCA-PEG NPs.

***In Vitro* Evaluation of TTCA-PEG NPs.** In this study, we aimed to demonstrate the potential of the developed TTCA-PEG NPs as drug delivery systems. To this end, we studied the loading of doxorubicin (DOX), selected as a model drug due to its straightforward handling, onto TTCA-PEG NPs.

The adsorption isotherm revealed that it is possible to achieve an adsorption of 72 μg of DOX per 1 mg of NPs. At a DOX concentration of 80 μg/mL, approximately 67.8% of DOX was adsorbed. Beyond this concentration, however, the solution's pH shifted to acidic, triggering nanoparticle aggregation as demonstrated in Figure 2J. In all later experiments we used NPs with 50 μg of DOX adsorbed per 1 mg of TTCA-PEG NPs. Then we demonstrated the enhanced release of DOX from TTCA-PEG NPs incubated with GSH and acetylcysteine (ACC) (93.3% and 67.9%, respectively) (Figure 4B), which occurs due to TTCA-PEG NP degradation resulting from disulfide bond cleavage in the presence of GSH and ACC. Furthermore, we conducted an evaluation of the time-dependent desorption of DOX from TTCA-PEG NPs. It is noteworthy that the addition of GSH resulted in the rapid degradation of NPs, leading to the fast release of DOX, in contrast to pure H_2O, where desorption occurred gradually over a 60 min period (Figure S7). The degradation of TTCA-PEG NPs in the presence of GSH was additionally confirmed by using SEM (Figure S4).

Additionally, we investigated the degradation of TTCA-PEG NPs by evaluating changes in the hydrodynamic diameter of NPs and the derived count rate using DLS after the incubation of TTCA-PEG NPs in various concentrations of ACC (Figure 4C). A steady decline in derived count rate was observed, with almost no change in hydrodynamic diameter until the ACC concentration reached 175 mM. Considering that disulfide bonds can exchange radicals, we assume that TTCA-PEG NPs maintain dynamic equilibrium with each other.[39] As such, the overall quantity of NPs decreases but their hydrodynamic diameter remains constant.

In vitro experiments of NPs as drug carriers were conducted on three cell lines: 4T1 murine breast cancer cells, A549 human lung carcinoma cells, and normal murine mesenchymal stromal cells (mMSCs). These cancer cell lines were chosen,

https://doi.org/10.1021/acs.nanolett.3c02933
Nano Lett. 2023, 23, 10811−10820

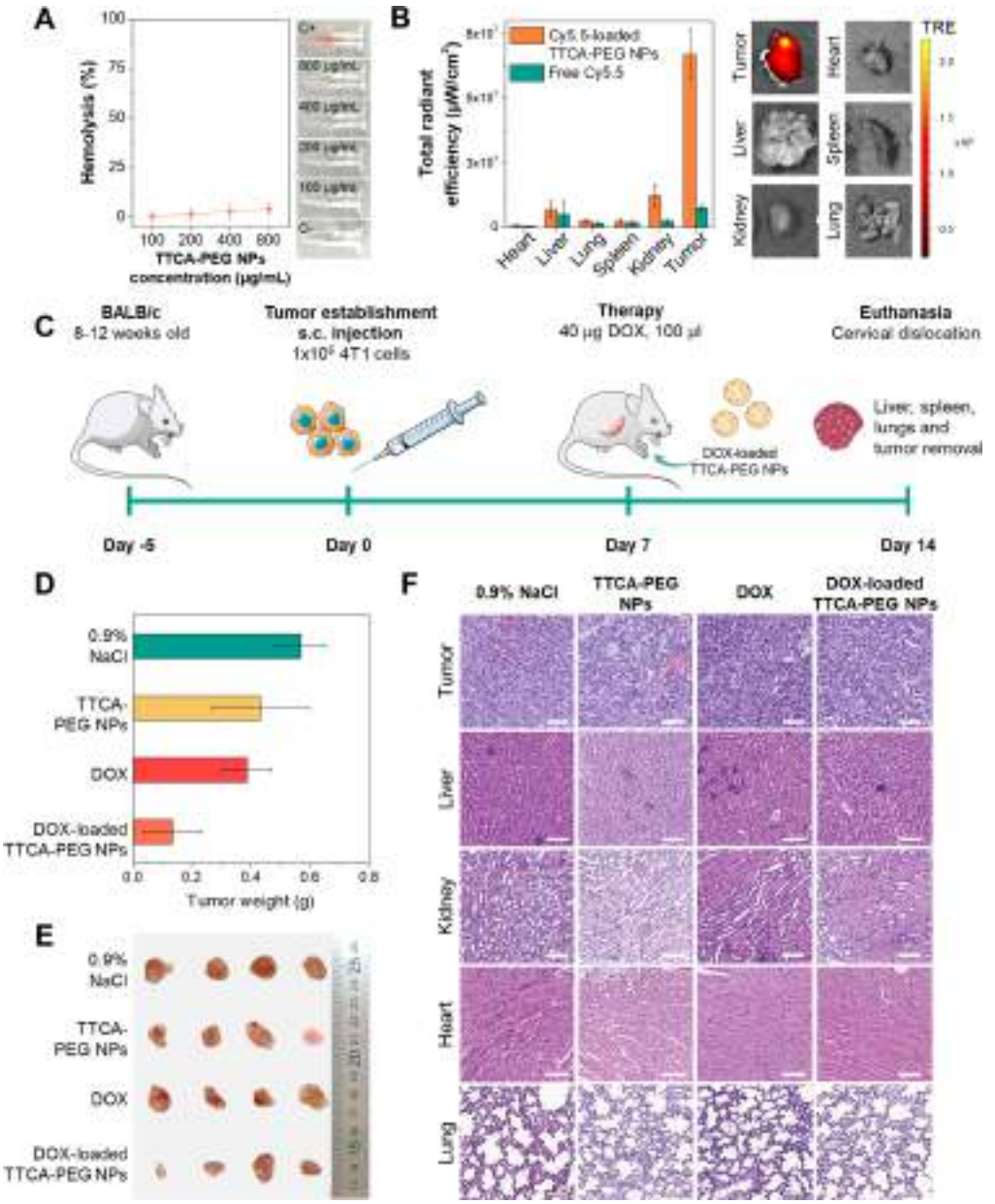

Figure 5. *In vivo* experiments. (A) Hemolysis assay of the TTCA-PEG NPs. (B) *Ex vivo* imaging of organs (tumor, liver, kidneys, heart, spleen, and lungs) harvested after the mice were euthanized after 6 h of intratumoral Cy5.5-loaded TTCA-PEG NPs or free Cy5.5 injection. Photos represent organs of a mouse that was injected with Cy5.5-loaded TTCA-PEG NPs. (C) Scheme of therapy and tumor growth estimation. (D) Tumor weight after the therapy after different types of treatment. (E) Digital photos of tumors extracted after the therapy. (F) H&E stained images of tumors and major organs (liver, kidney, heart, lungs) after therapy. To further investigate the therapeutic effect, tumor sections from euthanized mice were prepared for hematoxylin and eosin (H&E) staining to observe cell morphology. Despite noticeable differences in tumor size and weight, we found no significant alteration of the tumor microenvironment depending on the type of treatment. All tumor tissues displayed aggressive invasive tumor growth, significant infiltration of surrounding tissues, numerous blood vessels with incomplete vasculature, and spontaneous mitosis. Upon examination, the major organs (heart, liver, lungs, and kidneys) showed no evident histological lesions, suggesting the biosafety of the TTCA-PEG NPs. The scale bar corresponds to 200 μm. All error bars represent the standard deviation determined from three independent assays. The graphic was prepared using modified art elements from Servier Medical Art, found at https://smart.servier.com, used under a Creative Commons Attribution 3.0 Unported License.

since they have different intracellular GSH concentrations, with A549 having a higher GSH content compared to 4T1.[40,41] To assess the cellular uptake and intracellular degradation of carriers, we loaded TTCA-PEG NPs with a fluorescent molecule, Rhodamine B (RhB), and estimated the association and internalization of NPs using flow cytometry and confocal laser scanning microscopy (CLSM), respectively (Figure 4D–F). 4T1 cells demonstrated higher cell uptake levels than A549 cells at lower concentrations of TTCA-PEG NPs (12.5 and 25 μg/mL), as verified with flow cytometry. Confocal images of A549 cells over a 72 h span show internalization and dissolution of TTCA-PEG NPs within the cells, releasing RhB.

The association of RhB-loaded TTCA-PEG NPs with 4T1 cells was evaluated by using flow cytometry. Incubation of cells overnight with varying concentrations of RhB-loaded TTCA-PEG NPs revealed that at a concentration higher than 25 μg/

https://doi.org/10.1021/acs.nanolett.3c02933
Nano Lett. 2023, 23, 10811−10820

mL more than 90% of cells were associated with NPs (Figure 4E,F).

Lastly, we evaluated the cytotoxicity of synthesized DOX-loaded TTCA-PEG NPs on both cancer cell lines in comparison to normal mMSCs. Notably, the TTCA-PEG NPs demonstrated no toxic effects on any of the cell lines. Interestingly, despite an equal drug concentration, the DOX-loaded TTCA-PEG NPs were less toxic than pure DOX (Figure 4G–I). This can be attributed to the fact that some NPs remained noninternalized, resulting in a smaller overall concentration of DOX in the cells.[42]

It should also be highlighted that evaluating cell viability can be challenging since commonly used methods, such as MTT and Alamar Blue, rely on the reduction of specific agents that TTCA-PEG NPs can also reduce, thus potentially skewing experimental results. Further complicating matters is the use of 7AAD or other fluorescent compounds typically used for flow cytometry LIVE/DEAD assays, as TTCA-PEG NPs associated with cells tend to adsorb these compounds, leading to false positives. Consequently, we opted to use Calcein AM to perform cell viability experiments (Figures S10–S12).

Overall, this *in vitro* assessment demonstrates the potential of TTCA-PEG NPs as a drug delivery system with promising results in terms of drug adsorption, release, cell uptake, and cytotoxicity.

Antitumor Activity of DOX-Loaded TTCA-PEG NPs. We further evaluated the potential of our developed NPs as cytotoxic agent carriers in a mouse model of breast cancer. Prior to the *in vivo* evaluation, we conducted a hemolysis assay to reveal the impact of the obtained TTCA-PEG NPs on human erythrocytes. The hemolysis percentage of red blood cells remained below 5% at all the tested concentrations (up to 800 μg/mL) (Figure 5A). Additionally, TTCA-PEG NPs remained stable in human blood plasma for over 24 h (Figure S2).

For *in vivo* validation, we used a 4T1 tumor-bearing BALB/c mouse model. The tumor was established by subcutaneous injection of 4T1 cells. First, we estimated the biodistribution of Cy5.5-loaded TTCA-PEG NPs using fluorescence bioimaging IVIS. Cy5.5 was chosen as a far-red fluorescent dye to enable visualization of NPs within tissues. Most of the NPs remained within the tumor tissues following 6 h after intratumoral injection (Figure 5B and Figure S13). Furthermore, TTCA-PEG NPs demonstrated significantly higher retention of Cy5.5 within the tumor in comparison to free molecules after 6 h.

The treatment was performed on animals divided into four groups (n = 6): (i) control with 0.9% NaCl, (ii) DOX (40 μg DOX, 100 μL), (iii) TTCA-PEG NPs (0.8 mg NPs, 100 μL), and (iv) DOX-loaded TTCA-PEG NPs (40 μg DOX, 0.8 mg NPs, 100 μL). The amount of DOX injected corresponds to the commonly used 2 mg/kg DOX dosage.[43] After tumor development, TTCA-PEG NPs were injected intratumorally since these NPs lack active targeting in their current form. The mice were subsequently sacrificed 7 days after the start of therapy, and the size and weight of tumors were examined. We evaluated the tumor weights and compared them to those from untreated mice (Figure 5C). The injection of TTCA-PEG NPs alone did not significantly inhibit tumor growth. Conversely, the injection of DOX inhibited the tumor growth by 32%. Most notably, the injection of DOX-loaded TTCA-PEG NPs resulted in a remarkable 67% tumor inhibition (Figure 5D,E). Higher tumor inhibition of DOX-loaded TTCA-PEG NPs can be attributed to a higher retention of DOX in the tumor compared to free DOX and subsequent release of the drug after internalization of NPs. Furthermore, the histological examination of major organs (Figure 5F) (heart, liver, lungs, and kidneys) revealed no evident histological lesions, indicating the biosafety of TTCA-PEG NPs. This was further confirmed by blood routine and blood biochemistry tests, which were performed after intravenous injection of TTCA-PEG NPs. The results demonstrated that physiological parameters remained well within reference values, without significant alterations (Figure S14 and Table S1). Overall, this underscores the potential of TTCA-PEG NPs as a drug delivery platform.

Our work describes the development of a novel TTCA-based redox-responsive drug delivery system that is both affordable and simple to synthesize. We have comprehensively explored how key synthesis parameters influence the properties of the resulting TTCA NPs. By introducing a PEG linker, we enhanced the stability of these nanoparticles in biological media, making them a promising platform for controlled drug release. The TTCA-PEG NPs demonstrated high DOX, and both *in vitro* and *in vivo* tests confirmed the nontoxic nature of these particles. We have demonstrated the capability of these synthesized NPs for drug delivery, both *in vitro* and *in vivo*, and we highlighted potential challenges that may arise when working with these carriers.

Although we demonstrated the efficient delivery of antitumor drugs, we postulate that this drug delivery system could have broader applications. The high surface thiol content makes these nanoparticles potentially suitable for nasal delivery of various compounds or the delivery of genetic material, building on the reported endosomal escape of similar redox-responsive systems. These prospects underline the versatility of the developed TTCA-PEG NPs and open exciting directions for future research. Overall, this work lays a solid foundation for future studies of this system and may lead to significant advancements in redox-responsive drug delivery systems.

■ ASSOCIATED CONTENT

Supporting Information

The Supporting Information is available free of charge at https://pubs.acs.org/doi/10.1021/acs.nanolett.3c02933.

All materials, methods, synthesis parameters for the nanoparticles, and additional chemical and structural characterizations, along with detailed descriptions of the employed methods (PDF)

■ AUTHOR INFORMATION

Corresponding Author

Oleksii Peltek − *School of Physics and Engineering, ITMO University, St. Petersburg 191002, Russian Federation;* orcid.org/0000-0002-1485-7000; Email: peltek.oleksii@gmail.com

Authors

Elena Kopoleva − *School of Physics and Engineering, ITMO University, St. Petersburg 191002, Russian Federation*

Maksim D. Lebedev − *Ivanovo State University of Chemical and Technology, Ivanovo 153000, Russian Federation*

Alisa Postovalova − *School of Physics and Engineering, ITMO University, St. Petersburg 191002, Russian Federation*

Anna Rogova − *School of Physics and Engineering, ITMO University, St. Petersburg 191002, Russian Federation*

Landysh Fatkhutdinova − *School of Physics and Engineering, ITMO University, St. Petersburg 191002, Russian Federation*
Olga Epifanovskaya − *RM Gorbacheva Research Institute, Pavlov University, St. Petersburg 191144, Russian Federation*
Alexander A. Goncharenko − *Ivanovo State University of Chemical and Technology, Ivanovo 153000, Russian Federation*
Arina V. Kremleva − *Institute of Advanced Data Transfer Systems, ITMO University, St. Petersburg 191002, Russian Federation*
Nadezhda Domracheva − *Saint-Petersburg Chemical-Pharmaceutical University, St. Petersburg 197376, Russian Federation*
Anton S. Bukatin − *Alferov University, St. Petersburg 194021, Russian Federation; Institute for Analytical Instrumentation of the Russian Academy of Sciences, St. Petersburg 198095, Russian Federation*
Albert R. Muslimov − *RM Gorbacheva Research Institute, Pavlov University, St. Petersburg 191144, Russian Federation; Alferov University, St. Petersburg 194021, Russian Federation; Almazov National Medical Research Centre, Ministry of Health of the Russian Federation, St. Petersburg 197341, Russian Federation*
Aleksandra Koroleva − *Saint Petersburg State University, St. Petersburg 199034, Russian Federation*
Evgeniy V. Zhizhin − *Saint Petersburg State University, St. Petersburg 199034, Russian Federation*
Kirill V. Lepik − *RM Gorbacheva Research Institute, Pavlov University, St. Petersburg 191144, Russian Federation*
Alexander S. Timin − *Laboratory of nano- and microencapsulation of biologically active substances, Peter The Great St. Petersburg Polytechnic University, St. Petersburg 195251, Russian Federation;* orcid.org/0000-0002-0276-7892
Mikhail V. Zyuzin − *School of Physics and Engineering, ITMO University, St. Petersburg 191002, Russian Federation;* orcid.org/0000-0002-5364-2635

Complete contact information is available at: https://pubs.acs.org/10.1021/acs.nanolett.3c02933

Author Contributions

▲E.K. and O.P. contributed equally to this paper

Funding

This work was supported by the Russian Science Foundation (Project No. 23-23-00317).

Notes

The authors declare no competing financial interest.

■ ACKNOWLEDGMENTS

The XPS studies were performed on the equipment of the Resource Center "Physical methods of surface investigation" of the Scientific Park of St. Petersburg University. We thank FMBA for histological analysis. The FTIR analysis was carried out on the equipment of Center for Shared Use of Scientific Equipment of the Ivanovo State University of Chemistry and Technology (ISUCT).

■ REFERENCES

(1) Raza, A.; Rasheed, T.; Nabeel, F.; Hayat, U.; Bilal, M.; Iqbal, H. Endogenous and Exogenous Stimuli-Responsive Drug Delivery Systems for Programmed Site-Specific Release. *Molecules* **2019**, *24* (6), 1117.
(2) Shi, Y.; Cardoso, R. M.; Van Nostrum, C. F.; Hennink, W. E. Anthracene Functionalized Thermosensitive and UV-Crosslinkable Polymeric Micelles. *Polym. Chem.* **2015**, *6* (11), 2048−2053.
(3) Shi, Y.; Van Den Dungen, E. T. A.; Klumperman, B.; Van Nostrum, C. F.; Hennink, W. E. Reversible Addition-Fragmentation Chain Transfer Synthesis of a Micelle-Forming, Structure Reversible Thermosensitive Diblock Copolymer Based on the *N* -(2-Hydroxy Propyl) Methacrylamide Backbone. *ACS Macro Lett.* **2013**, *2* (5), 403−408.
(4) Sun, J.; Zhang, Y.; Chen, Z.; Zhou, J.; Gu, N. Fibrous Aggregation of Magnetite Nanoparticles Induced by a Time-Varied Magnetic Field. *Angew. Chem., Int. Ed.* **2007**, *46* (25), 4767−4770.
(5) Chen, Z.; Yin, J.-J.; Zhou, Y.-T.; Zhang, Y.; Song, L.; Song, M.; Hu, S.; Gu, N. Dual Enzyme-like Activities of Iron Oxide Nanoparticles and Their Implication for Diminishing Cytotoxicity. *ACS Nano* **2012**, *6* (5), 4001−4012.
(6) Mura, S.; Nicolas, J.; Couvreur, P. Stimuli-Responsive Nanocarriers for Drug Delivery. *Nat. Mater.* **2013**, *12* (11), 991−1003.
(7) Paris, J. L.; Cabañas, M. V.; Manzano, M.; Vallet-Regí, M. Polymer-Grafted Mesoporous Silica Nanoparticles as Ultrasound-Responsive Drug Carriers. *ACS Nano* **2015**, *9* (11), 11023−11033.
(8) Ding, H.; Tan, P.; Fu, S.; Tian, X.; Zhang, H.; Ma, X.; Gu, Z.; Luo, K. Preparation and Application of PH-Responsive Drug Delivery Systems. *J. Controlled Release* **2022**, *348*, 206−238.
(9) Lock, L. L.; Tang, Z.; Keith, D.; Reyes, C.; Cui, H. Enzyme-Specific Doxorubicin Drug Beacon as Drug-Resistant Theranostic Molecular Probes. *ACS Macro Lett.* **2015**, *4* (5), 552−555.
(10) Nguyen, M. M.; Carlini, A. S.; Chien, M.-P.; Sonnenberg, S.; Luo, C.; Braden, R. L.; Osborn, K. G.; Li, Y.; Gianneschi, N. C.; Christman, K. L. Enzyme-Responsive Nanoparticles for Targeted Accumulation and Prolonged Retention in Heart Tissue after Myocardial Infarction. *Adv. Mater.* **2015**, *27* (37), 5547−5552.
(11) Guo, X.; Cheng, Y.; Zhao, X.; Luo, Y.; Chen, J.; Yuan, W.-E. Advances in Redox-Responsive Drug Delivery Systems of Tumor Microenvironment. *J. Nanobiotechnol* **2018**, *16* (1), 74.
(12) Kanjilal, P.; Dutta, K.; Thayumanavan, S. Thiol-Disulfide Exchange as a Route for Endosomal Escape of Polymeric Nanoparticles. *Angew. Chem.* **2022**, *134* (37), e202209227.
(13) Yu, Z.-Q.; Sun, J.-T.; Pan, C.-Y.; Hong, C.-Y. Bioreducible Nanogels/Microgels Easily Prepared via Temperature Induced Self-Assembly and Self-Crosslinking. *Chem. Commun.* **2012**, *48* (45), 5623.
(14) Han, D.; Tong, X.; Zhao, Y. Block Copolymer Micelles with a Dual-Stimuli-Responsive Core for Fast or Slow Degradation. *Langmuir* **2012**, *28* (5), 2327−2331.
(15) Gasparini, G.; Bang, E.-K.; Montenegro, J.; Matile, S. Cellular Uptake: Lessons from Supramolecular Organic Chemistry. *Chem. Commun.* **2015**, *51* (52), 10389−10402.
(16) Aleksanian, S.; Khorsand, B.; Schmidt, R.; Oh, J. K. Rapidly Thiol-Responsive Degradable Block Copolymer Nanocarriers with Facile Bioconjugation. *Polym. Chem.* **2012**, *3* (8), 2138.
(17) Huo, M.; Yuan, J.; Tao, L.; Wei, Y. Redox-Responsive Polymers for Drug Delivery: From Molecular Design to Applications. *Polym. Chem.* **2014**, *5* (5), 1519−1528.
(18) O'Reilly, R. K.; Hawker, C. J.; Wooley, K. L. Cross-Linked Block Copolymer Micelles: Functional Nanostructures of Great Potential and Versatility. *Chem. Soc. Rev.* **2006**, *35* (11), 1068.
(19) Siegwart, D. J.; Oh, J. K.; Matyjaszewski, K. ATRP in the Design of Functional Materials for Biomedical Applications. *Prog. Polym. Sci.* **2012**, *37* (1), 18−37.
(20) Boyer, C.; Bulmus, V.; Davis, T. P.; Ladmiral, V.; Liu, J.; Perrier, S. Bioapplications of RAFT Polymerization. *Chem. Rev.* **2009**, *109* (11), 5402−5436.
(21) Fu, W.; Huang, Z. One-Pot Synthesis of a Two-Dimensional Porous Fe_3O_4/Poly($C_3N_3S_3$) Network Nanocomposite for the Selective Removal of Pb(II) and Hg(II) from Synthetic Wastewater. *ACS Sustainable Chem. Eng.* **2018**, *6* (11), 14785−14794.
(22) Fernandez-Francos, X.; Konuray, A.-O.; Belmonte, A.; De la Flor, S.; Serra, A.; Ramis, X. Sequential Curing of Off-Stoichiometric

Thiol-Epoxy Thermosets with a Custom-Tailored Structure. *Polym. Chem.* **2016**, *7* (12), 2280−2290.
(23) Konuray, A. O.; Fernández-Francos, X.; Ramis, X. Analysis of the Reaction Mechanism of the Thiol-Epoxy Addition Initiated by Nucleophilic Tertiary Amines. *Polym. Chem.* **2017**, *8* (38), 5934−5947.
(24) Kim, J.; Nam, H. Y.; Kim, T.; Kim, P.-H.; Ryu, J.; Yun, C.-O.; Kim, S. W. Active Targeting of RGD-Conjugated Bioreducible Polymer for Delivery of Oncolytic Adenovirus Expressing ShRNA against IL-8 MRNA. *Biomaterials* **2011**, *32* (22), 5158−5166.
(25) Huang, X.; Yang, J.; Wang, J.; Bi, J.; Xie, C.; Hao, H. Design and Synthesis of Core-Shell Fe3O4@PTMT Composite Magnetic Microspheres for Adsorption of Heavy Metals from High Salinity Wastewater. *Chemosphere* **2018**, *206*, 513−521.
(26) Skotheim, T. A.; Yang, X. Q.; Xue, K. H.; Lee, H. S.; McBreen, J.; Lu, F. X-Ray Absorption Studies on Organo-Disulfide Redox Cathodes. *Electrochim. Acta* **1992**, *37* (9), 1635−1637.
(27) Zeng, S.; Li, L.; Xie, L.; Zhao, D.; Zhou, N.; Wang, N.; Chen, S. Graphene-Supported Highly Crosslinked Organosulfur Nanoparticles as Cathode Materials for High-Rate, Long-Life Lithium-Sulfur Battery. *Carbon* **2017**, *122*, 106−113.
(28) Danehy, J. P.; Doherty, B. T.; Egan, C. P. Oxidation of Organic Divalent Sulfur by Iodine. II. Equilibrating Thiol-Iodine-Disulfide-Hydrogen Iodide System in Acetic Acid and Evidence for Sulfenyl Iodide Intermediates. *J. Org. Chem.* **1971**, *36* (17), 2525−2530.
(29) Dakwar, G. R.; Zagato, E.; Delanghe, J.; Hobel, S.; Aigner, A.; Denys, H.; Braeckmans, K.; Ceelen, W.; De Smedt, S. C.; Remaut, K. Colloidal Stability of Nano-Sized Particles in the Peritoneal Fluid: Towards Optimizing Drug Delivery Systems for Intraperitoneal Therapy. *Acta Biomaterialia* **2014**, *10* (7), 2965−2975.
(30) Kim, D.; Chae, M. K.; Joo, H. J.; Jeong, I.; Cho, J.-H.; Lee, C. Facile Preparation of Zwitterion-Stabilized Superparamagnetic Iron Oxide Nanoparticles (ZSPIONs) as an MR Contrast Agent for in Vivo Applications. *Langmuir* **2012**, *28* (25), 9634−9639.
(31) Zyuzin, M. V.; Honold, T.; Carregal-Romero, S.; Kantner, K.; Karg, M.; Parak, W. J. Influence of Temperature on the Colloidal Stability of Polymer-Coated Gold Nanoparticles in Cell Culture Media. *Small* **2016**, *12* (13), 1723−1731.
(32) Brändle, A.; Khan, A. Thiol-Epoxy 'Click' Polymerization: Efficient Construction of Reactive and Functional Polymers. *Polym. Chem.* **2012**, *3* (12), 3224.
(33) Kolate, A.; Baradia, D.; Patil, S.; Vhora, I.; Kore, G.; Misra, A. PEG — A Versatile Conjugating Ligand for Drugs and Drug Delivery Systems. *J. Controlled Release* **2014**, *192*, 67−81.
(34) Drożdżewski, P.; Malik, M.; Kopel, P.; Bieńko, D. C. Normal Vibrations and Vibrational Spectra of Trithiocyanuric Acid in Its Natural, Deuterated, Anionic and Metal Coordinated Forms. *Polyhedron* **2022**, *220*, 115819.
(35) Maity, P.; Kasisomayajula, S.; Parameswaran, V.; Basu, S.; Gupta, N. Improvement in Surface Degradation Properties of Polymer Composites Due to Pre-Processed Nanometric Alumina Fillers. *IEEE Trans. Dielect. Electr. Insul.* **2008**, *15* (1), 63−72.
(36) Ko, D.; Lee, J. S.; Patel, H. A.; Jakobsen, M. H.; Hwang, Y.; Yavuz, C. T.; Hansen, H. C. B.; Andersen, H. R. Selective Removal of Heavy Metal Ions by Disulfide Linked Polymer Networks. *Journal of Hazardous Materials* **2017**, *332*, 140−148.
(37) Kim, H.; Lee, J.; Ahn, H.; Kim, O.; Park, M. J. Synthesis of Three-Dimensionally Interconnected Sulfur-Rich Polymers for Cathode Materials of High-Rate Lithium-Sulfur Batteries. *Nat. Commun.* **2015**, *6* (1), 7278.
(38) Xue, J.; Qu, Y.; Chen, Y.; Zhang, C.; Bu, X. Effective Sulfide Flotation of Cerussite by Using Trithiocyanuric Acid as a Novel Sulfurizing Reagent. *Minerals Engineering* **2023**, *198*, 108087.
(39) Altinbasak, I.; Kocak, S.; Sanyal, R.; Sanyal, A. Fast-Forming Dissolvable Redox-Responsive Hydrogels: Exploiting the Orthogonality of Thiol-Maleimide and Thiol-Disulfide Exchange Chemistry. *Biomacromolecules* **2022**, *23* (9), 3525−3534.
(40) Zhu, C.; Hu, W.; Wu, H.; Hu, X. No Evident Dose-Response Relationship between Cellular ROS Level and Its Cytotoxicity - a Paradoxical Issue in ROS-Based Cancer Therapy. *Sci. Rep* **2014**, *4* (1), 5029.
(41) Tobwala, S.; Fan, W.; Hines, C. J.; Folk, W. R.; Ercal, N. Antioxidant Potential of Sutherlandia Frutescens and Its Protective Effects against Oxidative Stress in Various Cell Cultures. *BMC Complement Altern Med.* **2014**, *14* (1), 271.
(42) Zhang, L.; Liu, Y.; Zhang, K.; Chen, Y.; Luo, X. Redox-Responsive Comparison of Diselenide Micelles with Disulfide Micelles. *Colloid Polym. Sci.* **2019**, *297* (2), 225−238.
(43) McRae Page, S.; Henchey, E.; Chen, X.; Schneider, S.; Emrick, T. Efficacy of PolyMPC-DOX Prodrugs in 4T1 Tumor-Bearing Mice. *Mol. Pharmaceutics* **2014**, *11* (5), 1715−1720.

NOTE ADDED AFTER ASAP PUBLICATION

This paper published November 21, 2023 with an error in the Supporting Information file. The file was replaced and the paper reposted on November 28, 2023.

https://doi.org/10.1021/acs.nanolett.3c02933
Nano Lett. 2023, 23, 10811−10820